Low-Cost Sub-Fractional Horsepower Brushless Direct Current Claw-Pole Machine Topology for Fan Applications

Stefan Leitner[1,2], Hannes Gruebler[1,2], Annette Muetze[1,2]
[1]Christian Doppler Laboratory for Brushless Drives for Pump and Fan Applications, Graz, Austria
[2]Electrical Drives and Machines Institute, Graz University of Technology, Graz, Austria

***Abstract*—As to mass-produced sub-fractional horsepower (hp) drives, non-optimal motor behavior is often accepted when cost can be reduced, provided that reliability is not compromised. This paper proposes a brushless direct current (BLDC) claw-pole motor design for a sub-fractional hp fan drive, improving motor behavior twofold: 1) reducing cogging torque ripple and 2) realizing a preferred rotational direction, with no increase in manufacturing cost. Dimensions are so small that specially shaped steel sheets can be used for the stator instead of injection molded parts. The proposed measures are considered at the stage of punching the stator steel sheets and subsequent deep drawing thereof to yield the desired claw shapes and stator yoke. The findings show that the proposed measures (skewing and air gap asymmetry) can significantly reduce the cogging torque and the total torque ripple and prevent the motor from friction-related standstill with no increase in manufacturing cost.**

***Keywords*—Bifilar winding; brushless motors; claw-pole; cogging torque; fans; torque measurement; torque ripple; skewing; sub-fractional horsepower.**

I. Introduction

Brushless direct current (BLDC) motors have become omnipresent in various fields of machine application and power levels owing to their advantageous traits like high power density, good controllability, low maintenance, and high efficiency [1]. The automotive sector is just one of many industries where BLDC drives have been substituting established motor concepts in the light of energy efficiency even for very low power (sub-fractional horsepower) applications [2].

Effectively, BLDC drives are electronically commutated synchronous machines with permanent magnet excitation. Ideally, the induced back-EMF is of trapezoidal shape, requiring block commutation to produce average output torque. Opposed to three-phase brushless AC motors, BLDC motors usually need position sensors (e.g., hall sensor, magnetic encoder) in order to energize the windings at the right time.

Claw-pole machines are often used in mass-produced low-cost applications. Unfortunately, they often have geometry-induced high leakage flux and eddy current losses. However, claw-pole machines are known for having reduced component count and it is easy to realize a high number of poles. Claw-pole generators – also known as alternators – have been successfully used in the auto industry for years, charging the car's battery system when the combustion engine is running. Yet, limited information is available on their BLDC motor pendants which, owing to their electronic commutation, do not require slip rings. A 22 W 8 pole claw-pole motor of inner rotor type for a pump application is studied in [3], while [4] focuses on a 6 kW high-speed 4 pole outer rotor claw-pole motor for an axial flow air compressor using soft magnetic composites (SMC) to reduce eddy currents.

This paper proposes a sub-fractional horsepower claw-pole motor design for a fan application, showing measures to influence and improve the motor behavior with no increase in manufacturing cost, which is crucial for mass production. The proposed fan is in the 1 W range and is of axial flow type. In order to achieve a high integration, it seems natural to combine the motor with the application, using an outer rotor. The drive is designed to have a minimum number of machine parts. The dimensions are so small that the claw-like stator parts can be realized through punching and deep drawing of steel sheets. Advantageous to this motor topology is the ease of realizing stator skewing, which is usually very hard to apply or uneconomical for motors of these aspect ratios.

A detailed Finite Element Analysis is performed with JMAG© [9] showing the impact of the proposed design improvements. Prototypes are built and used to verify selected simulation results, i.e., the reduction in cogging torque peak values through stator claw skewing. Unlike [10], due to the small dimensions of the proposed motor drive, the cogging torque is measured utilizing the lever arm, attaching a weight to the rotor system.

The rest of the paper is divided into the following sections: Section II reviews the claw-pole motor topology and working principle, Section III presents the proposed design improvements, Section IV shows simulation results, Section V validates the design improvements experimentally, and Section VI concludes the findings of the paper.

The financial support by the Austrian Federal Ministry of Science, Research, and Economy and the National Foundation for Research, Technology, and Development is gratefully acknowledged.

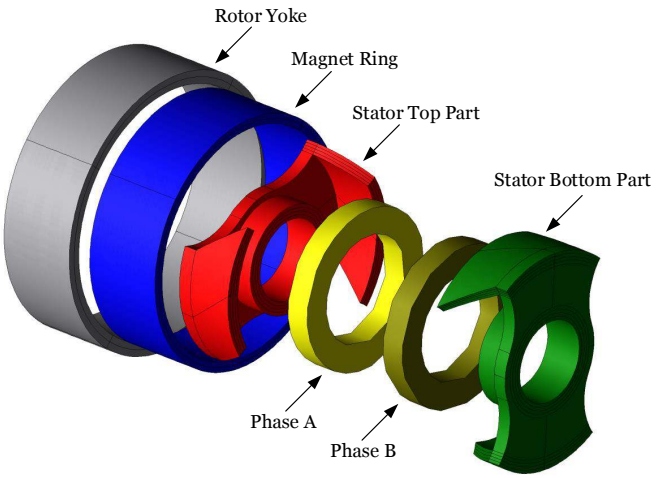

Fig. 1. 3D exploded view of the designed claw-pole motor model using Finite Element Analysis software JMAG© (from left to right: rotor yoke, magnet ring, stator top part, phases A and B of the bifilar field winding, and stator bottom part).

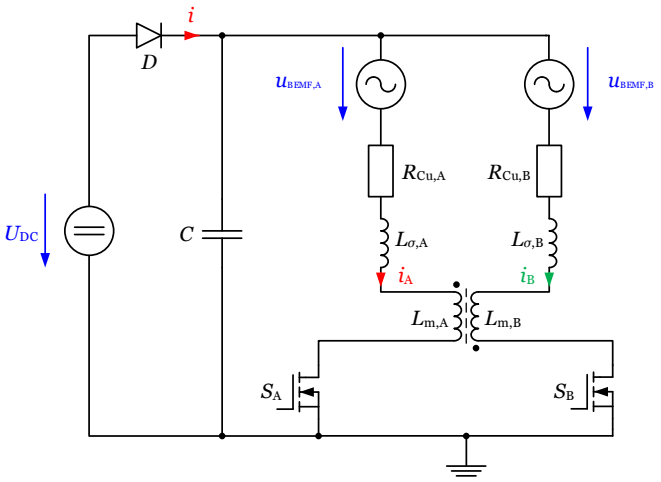

Fig. 2. Inverter circuit of the single-phase BLDC motor with bifilar stator winding and outer PM rotor.

II. Claw-Pole Motor Structure and Working Principle

This section briefly reviews the structure and working principle of claw-pole drives as they provide the context of the proposed design modifications when compared with conventional topologies. Notably, the drawbacks of the established design that the proposed design overcomes are high torque ripple, which often results in acoustic noise, friction-related standstill, and potential false start into the wrong direction. Section III discusses how to remedy said shortcomings.

Fig. 1 shows an exploded view of the proposed claw-pole BLDC motor consisting of an outer 4-pole PM rotor and a concentrated bifilar field winding housed by a bobbin and two specially shaped stator parts. Fig. 2 shows the inverter circuit of the proposed claw-pole BLDC motor. To reduce the number of power electronic components, a bifilar winding is chosen over a unifilar one. The concentrated bifilar field winding is energized by use of power electronic switches (S_A and S_B) driving flux through both stator parts, where one becomes a south and the other a north pole. Owing to the specially shaped stator parts, the flux distribution in this type of motor is three-dimensional.

Fig. 3(a) shows the conventional stator part punching layout for such a sub-fractional hp claw-pole motor when neither skewing nor air gap asymmetry is realized. The parameters r_2 and r_3 are the inner and outer radii of the final stator part, r_1 and r_4 determine the lengths of the deep drawn parts in z-direction displayed as hatched regions, the stator claw width $w_\mathrm{claw} = r_4 - r_3$, the stator yoke width $w_\mathrm{s,yoke} = r_2 - r_1$, w_stat is the stator width, and φ_pole is the pole angle. The parameter φ represents the circumferential angle in mechanical degrees.

In general, small machines often suffer from high torque ripples [5] (up to 100 % of torque peak value) which can cause friction-related standstill at low speed or can cause the motor to run up into the wrong direction. In sub-fractional hp machines, unlike air gap asymmetry, due to small dimensions and undesirable aspect ratios, it is often neither economical nor possible to apply skewing on the rotor or stator to reduce cogging torque [6].

In contrast to existing designs [4], this paper proposes a special stator claw-pole design allowing for the realization of stator claw skewing, when the steel sheets are punched and subsequently deep drawn, to reduce cogging torque significantly. The design is presented in the next section. In addition, it is shown how to also implement air gap asymmetry, which can change the cogging torque waveform but can help prevent the motor from friction-related standstill.

III. Claw-Pole Motor Design Improvements

A. Design of Skewing

In this subsection, a special sub-fractional hp claw-pole motor design is proposed where skewing can easily be included at the stage of punching the steel sheets and subsequent deep drawing thereof. As widely known, skewing can reduce cogging torque, which is often the reason for acoustic noise in a machine.

Fig. 3(b) shows how to realize stator claw skewing from the conventional design shown in Fig.3(a), where ξ_skew is the skewing angle in mechanical degrees, d_skew is the horizontal displacement, w_claw is the claw width, and r_3 is the outer stator radius. The optimal skewing angle $\xi_\mathrm{skew,opt}$ can be calculated from the pole pitch τ_p and the pole angle φ_pole:

$$\begin{aligned}\xi_\mathrm{skew,opt} &= \tau_p - \varphi_\mathrm{pole} \\ &= \frac{360^\circ}{2p} - \varphi_\mathrm{pole},\end{aligned} \tag{1}$$

where p is the number of stator pole pairs. The horizontal displacement d_skew can be calculated from w_claw and ξ_skew:

$$d_\mathrm{skew} = w_\mathrm{claw} \tan(\xi_\mathrm{skew}). \tag{2}$$

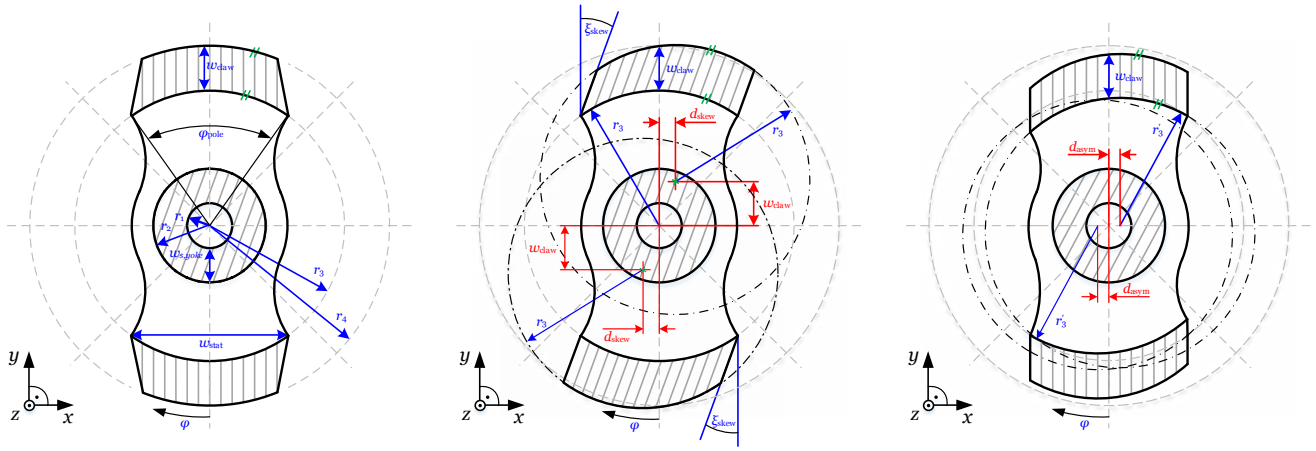

(a) Conventionally punched design. (b) Realization of skewed stator claws. (c) Realization of air gap asymmetry.

Fig. 3. Steel sheet layout for punching and subsequent deep drawing (deep drawn areas are hatched).

The two stator counterparts need to be manufactured with mirror-symmetry and, depending on the skewing angle, their main axes of symmetry need to be displaced by an angle other than $90°$ to yield constant distances between the skewed stator claws. On the downside, when skewing is applied, the two stator parts are not identical anymore and two different punching tools are necessary. However, the skewed stator claws can help realize a preferred rotational direction.

B. Design of Air Gap Asymmetry

In this subsection, it is shown how to implement air gap asymmetry which can prevent the rotor from friction-related standstill and at the same time reduce the output torque ripple. By adding air gap asymmetry, the radial reluctance varies along one stator pole circumferentially, causing a displacement of the magnetic symmetry line. When the rotor is released from its initial position, it will automatically rotate towards the new magnetic symmetry line. This way, the zero-positions of both the cogging torque (no-load condition) and the alignment torque (load condition) do not coincide and zero-torque positions of the output torque are avoided.

Fig. 3(c) shows how to realize air gap asymmetry using the stator width w_{stat}, the displacement d_{asym}, and the eccentric radius r_3'. Utilizing trigonometric identities, the stator width w_{stat}, the displacement d_{asym}, and the radius r_3' can be calculated from the pole angle φ_{pole}, the outer radius r_3, and the desired circumferential change in air gap $\Delta\delta$ as follows:

$$w_{\text{stat}} = 2\, r_3 \sin\left(\frac{\varphi_{\text{pole}}}{2}\right), \tag{3a}$$

$$d_{\text{asym}} = \frac{w_{\text{stat}}}{2} - \sqrt{\frac{w_{\text{stat}}^2}{4} - \Delta\delta^2}, \tag{3b}$$

$$r_3' = \sqrt{r_3^2 - \frac{w_{\text{stat}}^2}{4} + \left(\frac{w_{\text{stat}}}{2} - d_{\text{asym}}\right)^2}. \tag{3c}$$

For the proposed drive studied in Section IV, skewing and air gap asymmetry are combined (Figs. 3(b) and (c)). However, for reasons of clarity a combined drawing of the steel sheet layout has been omitted.

IV. Simulation Results

This section shows performance results of the proposed claw-pole BLDC drive with respect to stator claw skewing and air gap asymmetry. As an accurate determination of the cogging torque waveform requires the finite-element method [7], a detailed Finite Element Analysis with JMAG© is performed to determine the effects of skewing and air gap asymmetry on selected motor quantities. Investigated are the (no-load) back-EMF (BEMF), cogging torque waveforms, and output torque waveforms under load condition for different skewing angles, with and without airgap asymmetry. The simulation results, for a motor where both skewing and air gap asymmetry are applied, are summarized in Table I.

Figs. 4(a) and (b) show the effects of skewing on BEMF and cogging torque waveforms for skewing angles ξ_{skew} of $0°$, $15°$, and $30°$ (no air gap asymmetry is implemented). As expected, the BEMF peak values in Fig. 4(a) slightly decrease when skewing is applied due to the reduced flux-time areas. However, Fig. 4(b) illustrates how skewing can significantly reduce the cogging torque. It should be noticed that both the BEMF and cogging torque waveforms show symmetry. Fig. 4(c) shows the output torque waveforms under load condition (the windings are energized) for said skewing angles, where the output torque waveform becomes smoother for increasing skewing angles (higher torque harmonics are demonstrably reduced). The average output torque is slightly reduced, showing a total output torque ripple of $100\,\%$ for all three skewing angles, since the zero-torque positions of both the cogging torque and the alignment torque coincide when air gap asymmetry is not implemented. In Fig. 4(c), red circles mark said positions of zero output torque where friction-related standstill can occur at low-speed operation.

As the next step, airgap asymmetry is introduced to shift the zero-crossings of the cogging torque away from those of the

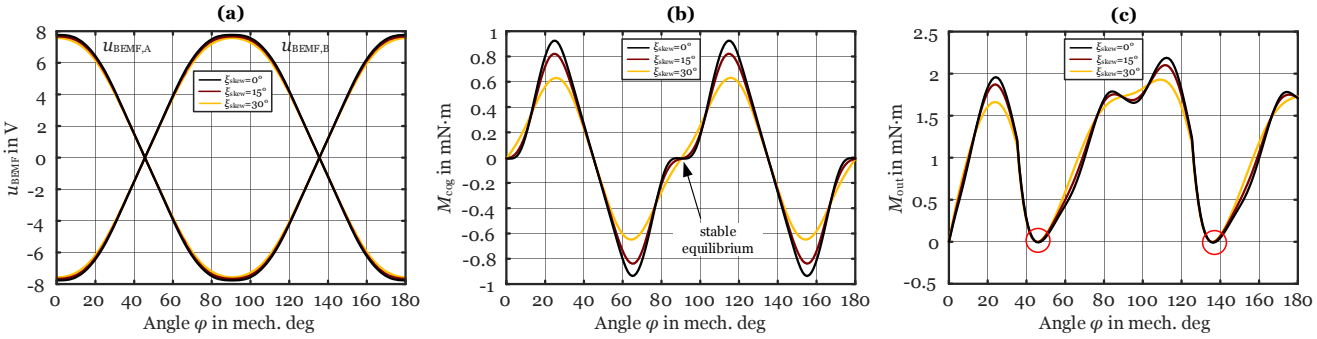

Fig. 4. Effects of skewing on (a) BEMF, (b) cogging torque, and (c) output torque waveforms for a change in air gap $\Delta\delta$ of 0.1 mm and skewing angles ξ_{skew} of 0°, 15°, and 30° (mech. deg).

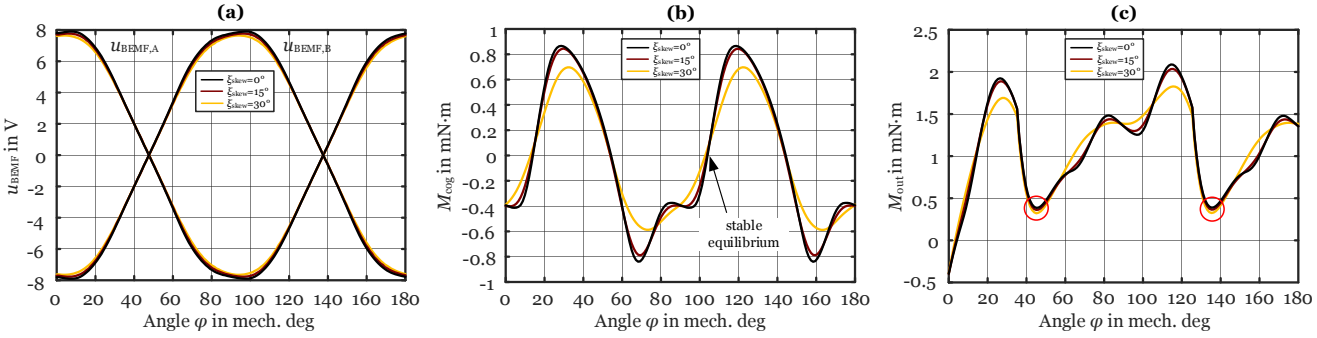

Fig. 5. Effects of both skewing and air gap asymmetry on (a) BEMF, (b) cogging torque, and (c) output torque waveforms for a change in air gap $\Delta\delta$ of 0.1 mm and skewing angles ξ_{skew} of 0°, 15°, and 30° (mech. deg).

TABLE I
EFFECTS OF SKEWING AND AIR GAP ASYMMETRY ON BEMF, COGGING TORQUE, AVERAGE OUTPUT TORQUE, AND TORQUE RIPPLE.

ξ_{skew} ° mech	$\hat{U}_{\mathrm{BEMF,A}}$ V	$\hat{U}_{\mathrm{BEMF,B}}$ V	$\Delta\overline{U}_{\mathrm{BEMF}}$ %	$\hat{M}^{+}_{\mathrm{cog}}$ mN·m	$\Delta\hat{M}^{+}_{\mathrm{cog}}$ %	$\hat{M}^{-}_{\mathrm{cog}}$ mN·m	$\Delta\hat{M}^{-}_{\mathrm{cog}}$ %	$\overline{M}_{\mathrm{out}}$ mN·m	$\hat{M}_{\mathrm{rip}}$ mN·m	$\Delta\hat{M}_{\mathrm{rip}}$ %	M_{rip} mN·m	ΔM_{rip} %
0	7.9	7.9	0	0.866	0	-0.839	0	1.135	2.09	0	1.7	0
15	7.77	7.77	1.65	0.845	2.42	-0.789	5.96	1.134	2.04	2.39	1.675	1.5
30	7.65	7.65	3.16	0.697	19.52	-0.587	30.04	1.131	1.826	12.63	1.496	12

alignment torque. Figs. 5(a) and (b) show the effects of both skewing and air gap asymmetry on BEMF and cogging torque waveforms for a change in air gap $\Delta\delta$ of 0.1 mm and skewing angles ξ_{skew} of 0°, 15°, and 30°. As expected, the BEMF peak values in Fig. 5(a) slightly decrease (by only 1.65 % and 3.16 %, see $\Delta\overline{U}_{\mathrm{BEMF}}$ in Table I) when skewing and air gap asymmetry are applied due to the reduced flux-time areas, similar to Figs. 4(a) and (b). The BEMF waveforms reflect the implemented air gap asymmetry as they are no longer symmetric. Fig. 5(b) illustrates the altered cogging torque waveform due to airgap asymmetry, where the shape of the positive and negative half-cycles differ as do their peak values. Notice that the saddle point in Fig. 4(b) (stable equilibrium position) moved to a position of nonzero cogging torque (see Fig. 5(b) for $\varphi \approx 90°$). For a skewing angle of 30° the described asymmetries are smoothed and the cogging torque peaks are reduced significantly. As can be seen, a skewing angle of 30° can reduce the positive and negative cogging torque peak values, $\hat{M}^{+}_{\mathrm{cog}}$ and $\hat{M}^{-}_{\mathrm{cog}}$, by about 20 % and 30 %, respectively (see $\Delta\hat{M}^{+}_{\mathrm{cog}}$ and $\Delta\hat{M}^{-}_{\mathrm{cog}}$ in Table I). Fig. 5(c) shows the output torque waveforms under load condition for said skewing angles and air gap asymmetry. Again, for increasing skewing angles, the output torque waveform becomes smoother and the higher torque harmonics are demonstrably reduced. In Fig. 5(c), the red circles mark the minimum values of the total output torque, showing that the torque ripple is smaller than 100 %. Hence, friction-related standstill at low speed is prevented. Table I lists the average output torque $\overline{M}_{\mathrm{out}}$, the output torque ripple M_{rip}, its peak value $\hat{M}_{\mathrm{rip}}$, and the reductions thereof, ΔM_{rip} and $\Delta\hat{M}_{\mathrm{rip}}$, for changing skewing angles. While the average output torque $\overline{M}_{\mathrm{out}}$ hardly changes, for $\xi_{\mathrm{skew}} = 30°$, the output torque ripple M_{rip} is successfully reduced by 12 %.

V. EXPERIMENTAL VERIFICATION

This section presents the experimental verification of selected simulation results presented in Section IV. The study

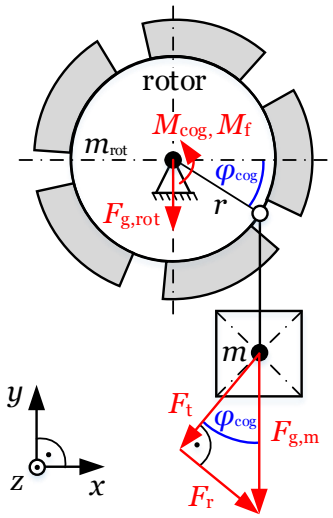

Fig. 6. Experimental test setup to measure the cogging torque.

Fig. 7. Manufactured stator parts (left: $\xi_{skew} = 30°$; right: $\xi_{skew} = 0°$).

system parameters are listed in Table II, the experimental test setup is shown in Fig. 6, and the manufactured stator parts are displayed in Fig. 7. Investigated is the effect of skewing on the cogging torque waveform.

A. Prototypes and Test Setup

This subsection describes the prototypes built and the prepared experimental test setup. It is shown how the cogging torque waveform of the prototypes is metrologically determined by attaching a mass to the rotor system.

Two prototype versions of the proposed claw-pole motor have been manufactured with skewing angles of $\xi_{skew} = 0°$ and $\xi_{skew} = 30°$, see Fig. 7. Due to economical reasons, the stator parts have been made utilizing CNC technology instead of punching and subsequent deep drawing of the stator parts. The used material is free-cutting steel 11SMnPb37. The rotor cup, consisting of a magnet ring, a rotor yoke, plastic fan blades, and a shaft, is kept in position by a slide bearing axially placed inside the stator parts.

As dynamic torque in sub-fractional hp motors is very hard to measure, static torque measurements, utilizing the lever arm of a force, are performed by attaching a mass to the rotor cup to verify the proposed design measures. The test setup is shown in Fig. 6, where r is the outer rotor cup radius, φ_{cog} is the angular displacement, M_{cog} is the cogging torque, M_f is the slide bearing's moment of friction, m is the attached

TABLE II
STUDY SYSTEM PARAMETERS

Parameter	Value	Parameter	Value
U_{DC}	8 V	B_r	0.42 T
$R_{Cu,A}$	16.4 Ω	$R_{Cu,B}$	16.4 Ω
N_A	208	N_B	208
r_2	3 mm	r_3	8 mm
$\Delta\delta$	0.072 mm	r_3'	7.928 mm
$w_{s,yoke}$	2.9 mm	w_{claw}	4.5 mm
r	11 mm	h_m	0.725 mm
φ_{pole}	72°	d_{asym}	0.12 mm

mass, m_{rot} is the mass of the rotor cup, $F_{g,rot}$ and $F_{g,m}$ are the gravitational forces of the rotor cup and the additional mass, respectively. $F_{g,m}$ can be separated into its tangential and radial components F_t and F_r, respectively. The thread used to attach the mass can be considered massless and the rotor cup can be assumed a rigid body with no elastic displacement when attaching the mass.

Starting from a stable equilibrium position (see Fig. 5(b)), a mass m is attached to the outer circumference of the rotor cup with a thread and increased successively while the angular displacement φ_{cog} is determined. The mass is increased so that the rotor leaves the stable equilibrium position, reaches the unstable equilibrium point, and exceeds it such that the rotor breaks loose reaching the next stable equilibrium position.

For the shown test setup, the slide bearing's moment of friction is a function of the attached mass m and can be calculated as follows (rigid body assumption):

$$M_f(m) = \mu_s[\, F_{g,rot} + F_{g,m}(m)] = \mu_s\,(m_{rot} + m)\, g_{Graz}, \quad (4)$$

where μ_s is the coefficient of static friction and g_{Graz} is the gravitational acceleration in Graz, Austria.

Both, the cogging torque and the moment of friction counteract the torque resulting from the mass that is attached to the rotor. In order to determine the cogging torque, the static friction of the slide bearing can be taken into account as follows:

$$\begin{aligned} M_{cog}(\varphi_{cog}) &= r\, F_t(\varphi_{cog}) - M_f(m) \\ &= r\, m\, g_{Graz} \cos(\varphi_{cog}) - \mu_s\,(m_{rot} + m)\, g_{Graz}. \end{aligned} \quad (5)$$

However, for the measurements, as neither a Stribeck curve nor a reliable coefficient of static friction of the used slide bearing–shaft combination are available, the influence of the friction is overcome by forcing the rotor cup to reach the respective equilibrium position through a damped oscillation, caused by an impulse of force.

B. Measuring Cogging Torque

This subsection discusses the cogging torque measurement of the described prototypes with skewing angles of $\xi_{skew} = 0°$

TABLE III
EXPERIMENTAL RESULTS – MOTOR WITH $\xi_{\text{SKEW}} = 0°$

m	φ_{cog}	M_{cog}	m	φ_{cog}	M_{cog}
g	°	mN·m	g	°	mN·m
8.1	−23	−0.8053	0	0	0
7.8	−22	−0.7842	0.7	1	0.0798
7.6	−21	−0.7624	1.6	2	0.1682
7.3	−20	−0.7400	2.4	4	0.2561
6.5	−18	−0.6648	3.2	5	0.3439
5.7	−16	−0.5869	4.0	6	0.4313
4.8	−14	−0.5066	4.8	8	0.5170
4.0	−12	−0.4242	5.7	9	0.6031
3.2	−9	−0.3410	6.5	12	0.6838
2.4	−7	−0.2548	7.3	14	0.7641
1.6	−4	−0.1679	7.6	15	0.7888
0.7	−1	−0.0798	7.8	16	0.8130

TABLE IV
EXPERIMENTAL RESULTS – MOTOR WITH $\xi_{\text{SKEW}} = 30°$

m	φ_{cog}	M_{cog}	m	φ_{cog}	M_{cog}
g	°	mN·m	g	°	mN·m
3.7	−17	−0.3858	0.7	2	0.0798
3.5	−15	−0.3616	1.6	5	0.1676
3.2	−12	−0.3377	2.4	9	0.2536
2.4	−9	−0.2536	3.2	14	0.3350
1.6	−6	−0.1674	4.0	18	0.4124
0.7	−3	−0.0797	4.3	20	0.4349
0	0	0	4.6	22	0.4561
			4.8	24	0.4760

and $\xi_{\text{skew}} = 30°$, respectively. The interaction of the magnets in the rotor cup with the stator parts is investigated with no windings energized. By increasing the mass attached to the rotor cup, shown in Fig. 6, the angular displacement φ_{cog} is measured and the cogging torque M_{cog} is calculated for each position according to (5), omitting the friction term M_{f}, since the influence of the friction is overcome as described in the previous section. The results are presented in Tables III and IV.

Fig. 8 shows the comparison of the simulated and measured cogging torque waveforms for skewing angles of $\xi_{\text{skew}} = 0°$ and $\xi_{\text{skew}} = 30°$, respectively. Abstracting from the saddle point in the negative half-cylce of the waveform (which can often not be seen in the measurements [11]), the experimental results are in general agreement with the simulation results. Yet, the measured cogging torque is lower than the simulated one (similar to [10], [12], [13]) for both skewing angles. These deviations may be attributed to slight differences in the actual and simulated 1) stator steel material, 2) residual flux densities of the magnet, and 3) stator geometry, and are subject to further investigations. However, it is evident from Tables III and IV, as well as from Fig. 8 that realizing a skewing angle of 30° for the proposed motor can reduce the cogging torque peaks down to about 50 % of the peak values of their counterpart with $\xi_{\text{skew}} = 0°$, confirming the effectiveness of the proposed measure.

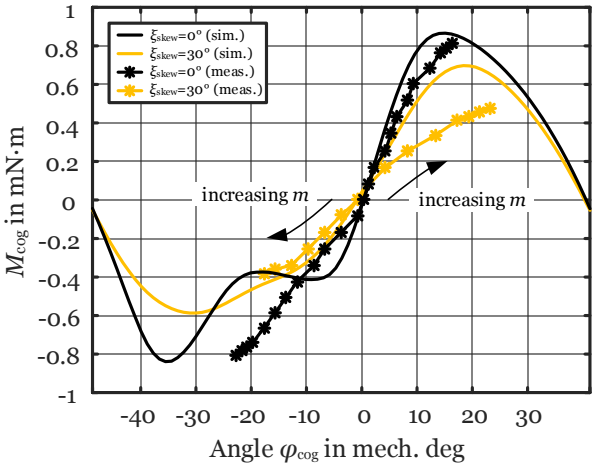

Fig. 8. Comparison between the simulated and measured cogging torque waveforms for $\xi_{\text{skew}} = 0°$ and $\xi_{\text{skew}} = 30°$.

VI. CONCLUSION

This paper proposes a simple sub-fractional hp claw-pole BLDC motor design, showing measures to easily improve the motor behavior with no increase in manufacturing cost, when punched and deep-drawn steel sheets are used, but significant improvement in motor behavior. With the proposed design, skewing and air gap asymmetry can easily be considered at the stage of punching and deep drawing the steel sheets. The findings show that skewing the stator claws by 30° can reduce the cogging torque significantly (while the BEMF peak values decrease only marginally and the average output torque hardly changes at all). Experimental results verify the simulation results and confirm the effectiveness of the proposed measures to improve the motor behavior.

REFERENCES

[1] Gui-Jia Su and J. W. McKeever, "Low-cost sensorless control of brushless DC motors with improved speed range," *IEEE Trans. Power Electron.*, vol. 19, no. 2, pp. 296–302, Mar. 2004.

[2] Chang-Liang Xia, Permanent Magnet Brushless DC Motor Drives and Controls. Wiley, Beijing: Science Press, 2012.

[3] H. Hembach, D. Gerling, and E. Nipp, "Analytical Design of a Claw-Pole Motor for Electrical Water Pump Applications," *2007 International Conference on Power Engineering, Energy and Electrical Drives*, Setubal, Portugal, 2007, pp. 174–179.

[4] Fengge Zhang, Hanyang Wei, Guangwei Liu, and Xueliang Bian, "Loss analysis of axial sectional claw pole high speed motor with permanent magnet outer rotor," *2013 International Conference on Electrical Machines and Systems (ICEMS)*, Busan, 2013, pp. 1345–1350.

[5] H. Le-Huy, R. Perret, and R. Feuillet, "Minimization of Torque Ripple in Brushless DC Motor Drives," *IEEE Trans. Ind. Appl.*, vol. IA-22, no. 4, pp. 748–755, Jul. 1986.

[6] Z. Q. Zhu and D. Howe, "Influence of Design Parameters on Cogging Torque in Permanent Magnet Machines," *IEEE Trans. Energy Convers.*, vol. 15, no. 4, pp. 407–412, Dec. 2000.
[7] J.R. Hendershot and T.J.E. Miller, "Basic Design Choices," in *Design of Brushless Permanent-Magnet Machines*, Florida, Motor Design Books LLC, 2010, ch. 3, sec. 3.5.12, pp. 107–108.
[8] H. Gruebler, S. Leitner, A. Muetze, and G. Schoener, "Improved Switching Strategy for a Single-Phase Brushless Direct Current Motor and its Impact on Motor Efficiency," IEEE International Electric Machines and Drives Conference (IEMDC), Miami, FL, 2017, pp. 1-6.
[9] JSOL Corporation, "Simulation Technology for Electromagnetical Design," http://www.jmag-international.com/, accessed on 23-11-2017.
[10] Z. Q. Zhu, "A simple method for measuring cogging torque in permanent magnet machines," IEEE Power and Energy Society General Meeting, Calgary, AB, 2009, pp. 1-4.
[11] Z. Q. Zhu, J. T. Chen, L. J. Wu, and D. Howe "Influence of Stator Asymmetry on Cogging Torque of Permanent Magnet Brushless Machines," *IEEE Trans. Mag.*, vol. 44, no. 11, pp. 3851–3854, Nov. 2008.
[12] Z. Q. Zhu and D. Howe, "Analytical prediction of the cogging torque in radial-field permanent magnet brushless motors," *IEEE Trans. Mag.*, vol. 28, no. 2, pp. 1371–1374, Mar. 1992.
[13] Z. Q. Zhu, S. Ruangsinchaiwanich, and D. Howe, "Synthesis of cogging-torque waveform from analysis of a single stator slot," *IEEE Trans. Ind. Appl.*, vol. 42, no. 3, pp. 650–657, May-Jun. 2006.